Direct N-body Simulations

⋆

Rainer Spurzem [a]

[a] *Astronomisches Rechen-Institut, Mönchhofstraße 12-14, D-69120 Heidelberg, Germany*

Abstract

Special high-accuracy direct force summation N-body algorithms and their relevance for the simulation of the dynamical evolution of star clusters and other gravitating N-body systems in astrophysics are presented, explained and compared with other methods. Other methods means here approximate physical models based on the Fokker-Planck equation as well as other, approximate algorithms to compute the gravitational potential in N-body systems. Questions regarding the parallel implementation of direct "brute force" N-body codes are discussed. The astrophysical application of the models to the theory of relaxing rotating and non-rotating collisional star clusters is presented, briefly mentioning the questions of the validity of the Fokker-Planck approximation, the existence of gravothermal oscillations and of rotation and primordial binaries.

1 Introduction

"The dynamical evolution of an isolated spherical system composed of very many mass points has an appealing simplicity. The Newtonian laws of motion are exact, and all average quantities are functions only of radial distance r and time t. Nevertheless, it is only recently, with the availability of fast computers, that a systematic understanding of how such systems develop through time has emerged. Since these idealized systems should provide a very good approximation for globular clusters in this and other galaxies, the theory of their development is an important part of astronomy as well as an interesting branch of theoretical particle dynamics." [77]

⋆ to appear in: Riffert H., Werner K. (eds), Computational Astrophysics, The Journal of Computational and Applied Mathematics (JCAM), Elsevier Press, Amsterdam.

Once celestial mechanics was one of the most important fields of astronomy. Nowadays astrophysics has become much wider in scope, including fields like stellar astrophysics and gas and plasma dynamics of interstellar matter. For some objects, however, the pure dynamics of gravitating mass points still provides an excellent description of the global dynamical evolution or gives at least the dominating background in which the gaseous or baryonic matter evolves. Such objects are, starting from the large scale, the entire universe itself, some evolutionary phases of galaxies and galactic nuclei, globular and open star clusters, and last but not least our planetary system. Globular star clusters are gas free systems with some 10^5 stars, orbiting around our own [14] and other galaxies [70].

This article aims at the complex interplay of thermodynamic processes like heat conduction and relaxation with the physics of self-gravitating systems and the stochastic nature of star clusters having finite particle number N, and the specific computational and physical models used for the numerical simulation of the dynamical evolution of star clusters under these processes on the computer. Globular clusters are a very good laboratory for relaxation processes in discrete particle systems, because their dynamical and relaxation timescales are well separated from each other and from the lifetime of the cluster and of the universe as a whole. In this article the methods appropriate to model their evolution are in the focus. Other kinds of N-body simulations are useful for example for hydrodynamics ("smoothed particle hydrodynamics"), galaxy dynamics ("collisionless systems") or cosmological N-body simulations of structure formation in the universe and are covered by other articles in this volume. The main distinction of those from the models presented here, is that the dynamics of systems dominated by two-body relaxation ("collisional systems") requires typically very high accuracies (typical energy error per crossing time $\Delta E/E < 10^{-5}$ or smaller) over very long physical integration times (thousands of crossing times). The term "collisional" here always refers to systems, whose evolution is influenced by relaxation through elastic two- or more-body encounters, *not* to physical collisions, where two stars collide and merge or disrupt each other. As a consequence of the high accuracy requirements for collisional N-body simulations, commonly known algorithms like the leap-frog time integration and the TREE-method to compute the gravitational potential of a particle distribution, are not efficient to use here; the use of high-order time integration schemes and "brute–force" algorithms to compute the potential are more efficient, as will be argued below.

This article is organized as follows: this introduction is followed by a section on the approximate models of self-gravitating collisional N-body systems, after which practical and theoretical aspects of the corresponding highly accurate direct N-body simulations are presented. Finally astrophysical applications of the methods and relevant questions under study are presented.

Let us begin with the definition of some useful time scales. A typical particle crossing time $t_{\rm cr}$ in a star cluster is

$$t_{\rm cr} = \frac{r_h}{\sigma_h} \ , \tag{1}$$

where r_h is the radius containing 50 % of the total mass and σ_h is a typical velocity associated with the root mean square random motion (velocity dispersion) taken at r_h. If virial equilibrium prevails, we have $\sigma_h^2 \approx GM_h/r_h$ (where the sign $\approx$ here and henceforth means "approximately equal" or "equal within an order of magnitude"), thus

$$t_{\rm cr} \approx \sqrt{\frac{r_h^3}{GM_h}} \ . \tag{2}$$

This is equal to the dynamical timescale, which is also used for example in the theory of stellar structure and evolution. Global dynamical adjustments of the system, like oscillations, are connected with this timescale. Taking the square of equation 2 yields $t_{\rm cr}^2 \approx r_h^3/(GM_h)$ which is related to Kepler's third law, because the orbital velocity in a Keplerian point mass potential has the same order of magnitude as the velocity dispersion in virial equilibrium.

Unlike most laboratory gases stellar systems are not usually in thermodynamic equilibrium, neither locally nor globally. Radii of stars are usually extremely small relative to the average interparticle distances of stellar systems (e.g. the radius of the sun is $r_\odot \approx 10^{10}$ cm, a typical distance between stars in our galactic neighbourhood is of the order of 10^{18}cm). Only under rather special conditions in the centres of galactic nuclei and during the short high-density core collapse phase of a globular cluster, stellar densities might become large enough that stars come close enough to each other to collide, merge or disrupt each other.

Therefore it is extremely unlikely under normal conditions that two stars touch each other during an encounter; encounters or collisions usually are elastic gravitative scatterings. Fairly generally the mean interparticle distance is large compared to $p_0 = Gm/\sigma^2$, which is the impact parameter for a 90^o deflection in a typical encounter of two stars of equal mass m, where the relative velocity at infinity is $\sqrt{2}\sigma$, with local 1D velocity dispersion σ. Thus most encounters are small-angle deflections. The relaxation time $t_{\rm rx}$ is defined as the time after which the root mean square velocity increment due to such small angle gravitative deflections is of the same order as the initial velocity dispersion of the system. We use the local relaxation time as defined by [49]:

$$t_{\rm rx} = \frac{9}{16\sqrt{\pi}} \frac{\sigma^3}{G^2 m \rho \ln(\gamma N)} \ . \tag{3}$$

G is the gravitational constant, ρ the mean stellar mass density, N the total particle number, and γ a parameter of order unity, which results from an integration over all possible impact parameters for a two-body encounter. Taking the linear system dimension as a maximum impact parameter yields $\gamma = 0.4$ [77]. Measurements in direct star by star evolutionary simulations of stellar systems are more in favour of $\gamma = 0.11$ [22,23], which is the value used throughout this article.

Assuming virial equilibrium a fundamental proportionality turns out:

$$\frac{t_{\rm rx}}{t_{\rm dyn}} \propto \frac{N}{\ln(\gamma N)} \ . \tag{4}$$

(cf. e.g. [77]). As a result, for very large N, dynamical equilibrium is attained much faster than thermodynamic equilibrium. If one assumes a purely kinetic temperature definition, it ensues that in star clusters the temperatures (or velocity dispersions) can remain different for different coordinate directions over many dynamical times. For example, in a spherical system the radial and tangential velocity dispersion would be different, which is denoted as anisotropy.

There are several reasons to believe that anisotropy is present and important for the dynamical evolution of astrophysical star clusters. Many observations are matched better by models including anisotropy [55], and all direct simulations exhibit the formation of anisotropy under very general conditions, independent of the underlying physical cause driving the system's evolution. [8] showed in the context of a gas dynamical model of star clusters, that isotropy remains only under very special conditions (linear profiles of velocities of mass and energy transport), and a similar study [36] gives the same result for axisymmetric collapsing gaseous systems.

2 Approximate Models

2.1 Fokker-Planck Approximation

Unfortunately, the direct simulation of such rich stellar systems as globular clusters with star-by-star modelling is not yet possible. The gap between the largest useful N-body models with particle numbers of the order of a few 10^4 particles and the median globular star cluster ($N \sim 5 \times 10^5$) can only be bridged at present by use of theory. There are two main classes of theory: (i) Fokker-Planck models, which are based on the Boltzmann equation of the kinetic theory of gases [13,72,29,15], and (ii) gas models [54,79,32], which can be thought of as a set of moment equations of the Fokker-Planck model.

These simplified models are the only detailed models which are directly applicable to large systems such as globular clusters. But their simplicity stems from many approximations and assumptions which are required in their formulation. Examples are the assumptions of spherical symmetry, which contradicts the asymmetry of the galactic tidal field, or statistical estimates of cross sections for the formation of close binaries by three-body or dissipative (tidal) two-body encounters, and for their subsequent gravitational interactions with field stars. Such processes play a dominant role to reverse core collapse of globular clusters, which otherwise would inevitably lead to a singular density profile with infinite density at the centre [9,19,41].

The Fokker-Planck approximation truncates the so–called B^{2}GKY hierarchy of kinetic equations (see [10]) at lowest order assuming that for most of the time all particles are uncorrelated with each other and only coupled via the smooth global gravitational potential. Correlations only play a role as a sequence of uncorrelated two-body encounters. Instead of determining a general correlation function one resorts to a phenomenological description of the effects of collisions by computing diffusion coefficients directly from the known solution of the two-body problems. Diffusion coefficients $D(\Delta v_i)$ and $D(\Delta v_i v_j)$ denote the average rate of change of v_i and $v_i v_j$ due to the cumulative effect of many small angle deflections during two-body encounters. Let m, $\vec{v}$ and m_f, $\vec{v_f}$ be the mass and velocity of a star from a test and field star distribution, respectively (both distributions can but need not to be the same). In Cartesian geometry the diffusion coefficients are defined by

$$D(\Delta v_i) = 4\pi G^2 m_f \ln\Lambda \frac{\partial h(\vec{v})}{\partial v_i} \quad ; \quad D(\Delta v_i v_j) = 4\pi G^2 m_f \ln\Lambda \frac{\partial^2 g(\vec{v})}{\partial v_i v_j} \quad ; \quad (5)$$

where f is the phase space density of stars (briefly: distribution function) and g, h are the Rosenbluth potentials defined in [76]

$$h(\vec{v}) = (m + m_f) \int \frac{f(\vec{v}_f)}{|\vec{v} - \vec{v}_f|} d^3\vec{v}_f \quad ; \quad g(\vec{v}) = m_f \int f(\vec{v}_f) |\vec{v} - \vec{v}_f| d^3\vec{v}_f \ . \quad (6)$$

Note that provided the distribution function f is given in terms of a convenient polynomial series as in Legendre polynomials the Rosenbluth potentials can be evaluated analytically to arbitrary order, as was seen already by [76], see for a modern rederivation and its use for star cluster dynamics [26,82]. With these results we can finally write down the local Fokker-Planck equation in its standard form for the Cartesian coordinate system of the v_i:

$$\frac{\partial f}{\partial t} + \vec{v}_i \frac{\partial f}{\partial \vec{r}_i} + \dot{\vec{v}}_i \frac{\partial f}{\partial \vec{v}_i} = \left(\frac{\delta f}{\delta t}\right)_{\rm enc} \quad ; \tag{7}$$

$$\left(\frac{\delta f}{\delta t}\right)_{\rm enc} = -\sum_{i=1}^{3} \frac{\partial}{\partial v_i}\Big[f(\vec{v})D(\Delta v_i)\Big] + \frac{1}{2}\sum_{i,j=1}^{3} \frac{\partial^2}{\partial v_i \partial v_j}\Big[f(\vec{v})D(\Delta v_i v_j)\Big] \ . \tag{8}$$

The subscript "enc" should refer to encounters, which are the driving force of two–body relaxation. Still Eq. 7 is a six-dimensional integro-differential equation; its direct numerical simulation in stellar dynamics can presently only be done by further simplification. First Jeans' theorem is applied and f transformed into a function of the classical integrals of motion of a particle in a potential under the given symmetry, as e.g. energy E and modulus of the angular momentum J^2 in a spherical potential or E and z-component of angular momentum J_z in axisymmetric coordinates. Thereafter the Fokker-Planck equation can be integrated over the accessible coordinate space for any given combination of constants of motion and the orbit-averaged Fokker-Planck equation ensues. By transformation from v_i to E and J and via the limits of the orbital integral the potential enters both implicitly and explicitly. In a two-step scheme alternatively solving the Poisson- and Fokker-Planck equation a direct numerical solution is obtained [12,15,85–87,18]. One of the main uncertainties in this method is that for non-spherical mass distributions the orbit structure in the system may depend on unknown non-classical third integrals of motion which are neglected.

2.2 Anisotropic Gaseous Model

The local Fokker-Planck equation Eq. 7 is utilized in another way for gaseous or conducting sphere models of star clusters. Integrating it over velocity space with varying powers of the velocity coordinates yields a system of equations in the spatial coordinates; the local approximation is used in the sense that the orbit structure of the system is not taken into account, diffusion coefficients and all other quantities are assumed to be well defined just as a function of the local quantities (density, velocity dispersions and so on). The system of moment equations is truncated in third order by a phenomenological equation of heat transfer. Such approach has been suggested by [56,33] and generalized to anisotropic systems by [8,54], and for a presentation of the recent model see e.g. [26]. In the following the derivation of the model equations is decribed.

2.2.1 The "Left Hand Sides"

In spherical symmetry, polar coordinates r θ, ϕ are used and t denotes the time. The vector $\vec{v} = (v_i), i = r, \theta, \phi$, denotes the velocity in a local Cartesian coordinate system at the spatial point r, θ, ϕ. For brevity $u = v_r$, $v = v_\theta$, $w = v_\phi$ is used. The distribution function f, which due to spherical symmetry is a function of r, t, u, $v^2 + w^2$ only, is normalized according to

$$\rho(r,t) = \int f(r, u, v^2 + w^2, t) du\, dv\, dw, \tag{9}$$

where $\rho(r,t)$ is the mass density; if m denotes the stellar mass, we get the particle density $n = \rho/m$. Then

$$\bar{u} = \int u f(r, u, v^2 + w^2, t) du\, dv\, dw, \tag{10}$$

is the bulk radial velocity of the stars. Note that for the analogously defined quantities $\bar{v}$ and $\bar{w}$ we have $\bar{v} = \bar{w} = 0$.

In order to go ahead to the anisotropic gaseous model equations we now turn back to the left hand side of the Fokker-Planck equation Eq. 7, which is the collisionless Boltzmann or Vlasov operator. For practical reasons we prefer for the left hand side local Cartesian velocity coordinates, whose axes are oriented towards the r, θ, ϕ coordinate space directions. With the Lagrange function

$$\mathcal{L} = \frac{1}{2}(\dot{r}^2 + r^2\dot{\theta}^2 + r^2 \sin^2\theta\, \dot{\phi}^2) - \Phi(r,t) \tag{11}$$

the Euler-Lagrange equations of motion for a star moving in the cluster potential Φ become:

$$\dot{u} = -\frac{\partial \Phi}{\partial r} + \frac{v^2 + w^2}{r} \quad ; \quad \dot{v} = -\frac{uv}{r} + \frac{w^2}{r \tan\theta} \quad ; \quad \dot{w} = -\frac{uw}{r} - \frac{vw}{r\tan\theta} \quad . \tag{12}$$

The complete local Fokker-Planck equation, derived from Eq. 7, attains the form

$$\frac{\partial f}{\partial t} + u\frac{\partial f}{\partial r} + \dot{u}\frac{\partial f}{\partial u} + \dot{v}\frac{\partial f}{\partial v} + \dot{w}\frac{\partial f}{\partial w} = \left(\frac{\delta f}{\delta t}\right)_{\rm enc} , \tag{13}$$

where the term subscribed by "enc" denotes the terms involving diffusion coefficients as in Eq. 8. Moments $\langle i, j, k\rangle$ of f are defined in the following way (all integrations range from $-\infty$ to ∞):

$$\langle 0,0,0\rangle := \rho = \int f du dv dw \quad ; \quad \langle 1,0,0\rangle := \bar{u} = \int u f du dv dw \tag{14}$$

$$\langle 2,0,0\rangle := p_r + \rho\bar{u}^2 = \int u^2 f du dv dw \tag{15}$$

$$\langle 0,2,0\rangle := p_\theta = \int v^2 f\,du\,dv\,dw \quad ; \quad \langle 0,0,2\rangle := p_\phi = \int w^2 f\,du\,dv\,dw \tag{16}$$

$$\langle 3,0,0\rangle := F_r + 3\bar{u}p_r + \bar{u}^3 = \int u^3 f\,du\,dv\,dw \tag{17}$$

$$\langle 1,2,0\rangle := F_\theta + \bar{u}p_\theta = \int uv^2 f\,du\,dv\,dw \tag{18}$$

$$\langle 1,0,2\rangle := F_\phi + \bar{u}p_\phi = \int uw^2 f\,du\,dv\,dw \ . \tag{19}$$

Note that the definitions of p_i and F_i are such that they are proportional to the random motion of the stars. Due to spherical symmetry we have $p_\theta = p_\phi =: p_t$ and $F_\theta = F_\phi =: F_t/2$. By $p_r = \rho\sigma_r^2$ and $p_t = \rho\sigma_t^2$ the random velocity dispersions are given, which are closely related to observables in globular star clusters and galaxies. It is convenient to define velocities of energy transport by

$$v_r = \frac{F_r}{3p_r} + u \quad ; \quad v_t = \frac{F_t}{2p_t} + u \ . \tag{20}$$

By multiplication of the Fokker-Planck equation 13 with various powers of u, v, w we get up to second order the following set of moment equations (for a detailed derivation in the here used variables see [78], bar for $\bar{u}$ dropped in the following):

$$\frac{\partial\rho}{\partial t} + \frac{1}{r^2}\frac{\partial}{\partial r}\left(r^2 u\rho\right) = 0 \tag{21}$$

$$\frac{\partial u}{\partial t} + u\frac{\partial u}{\partial r} + \frac{GM_r}{r^2} + \frac{1}{\rho}\frac{\partial p_r}{\partial r} + 2\frac{p_r - p_t}{\rho r} = 0 \tag{22}$$

$$\frac{\partial p_r}{\partial t} + \frac{1}{r^2}\frac{\partial}{\partial r}\left(r^2 u p_r\right) + 2p_r\frac{\partial u}{\partial r} + \frac{1}{r^2}\frac{\partial}{\partial r}\left(r^2 F_r\right) - \frac{2F_t}{r} = \left(\frac{\delta p_r}{\delta t}\right)_{\rm enc,bin3} \tag{23}$$

$$\frac{\partial p_t}{\partial t} + \frac{1}{r^2}\frac{\partial}{\partial r}\left(r^2 u p_t\right) + 2\frac{p_t u}{r} + \frac{1}{2}\frac{1}{r^2}\frac{\partial}{\partial r}\left(r^2 F_t\right) + \frac{F_t}{r} = \left(\frac{\delta p_t}{\delta t}\right)_{\rm enc,bin3} . \tag{24}$$

The terms labeled with “enc” and “bin3” symbolically denote the collisional terms resulting from the moments of the right hand side of the Fokker-Planck equation (Eq. 8) and an energy generation by formation and hardening of three body encounters. Both will be discussed below. With the definition of the mass M_r contained in a sphere of radius r

$$\frac{\partial M_r}{\partial r} = 4\pi r^2\rho \tag{25}$$

the set of Eqs. 22–24 is equivalent to gasdynamical equations coupled with Poisson’s equation. Since moment equations of order n contain moments of order $n+1$, it is necessary to close the system of the above equations by an independent closure relation. Here we choose the heat conduction closure, which consists of a phenomenological ansatz in analogy to gas dynamics. It was first used (restricted to isotropy) by [56]. It is assumed that heat transport is proportional to the temperature gradient, where we use for the temperature gradient an average velocity dispersion $\sigma^2 = (\sigma_r^2 + 2\sigma_t^2)/3$ and assume $v_r = v_t$ (this latter closure was first introduced by [8]). Therefore, the last two equations to close our model are

$$v_r - u + \frac{\lambda}{4\pi G \rho t_{\rm rx}} \frac{\partial \sigma^2}{\partial r} = 0 \quad ; \quad v_r = v_t \ . \tag{26}$$

With Eqs. 22–24, 25, and 26 we have now seven equations for our seven dependent variables M_r, ρ, u, p_r, p_t, v_r, v_t.

2.2.2 Binary Heating

It was already early realized that in a star cluster with single stars under high density conditions, one or more strongly bound binaries form, which could dominate the further evolution [35,4]. This is a contradiction to the basic assumption underlying the Fokker-Planck equation, that the only correlations in the system are those produced by a sequence of uncorrelated small-angle gravitational encounters. Nevertheless [9] introduced a phenomenological heat source into their gaseous model equations, in order to describe the input of random kinetic energy ("heat") to the cluster by formation and hardening of so-called three-body binaries. The ansatz for the functional form of the heating term has been clarified and more thoroughly discussed by [27,34]. They describe a simple estimate for the rate of formation of binaries by close three-body encounters of single stars; in subsequent superelastic scatterings between the formed binary and field stars the binary will on average become harder, provided its binding energy is large compared to the mean temperature of the surrounding single stars. Surplus kinetic energy taken from the gravitational binding energy of the binary members goes to the field star and thus provides a heating source for the core of the cluster. There is an upper limit of the binary binding energy given by the condition that the recoil on the binary in a typical superelastic scattering due to conservation of linear momentum in the process leads to escape of the binary. As a result each binary after its formation supplies a certain amount of energy by three-body encounters to the system until it escpes. The resulting heating term is (isotropic binary heating assumed):

$$\left(\frac{\delta p_r}{\delta t}\right)_{\rm bin3} = \frac{2}{3} C_b m n^3 \sigma^3 \left(\frac{Gm}{\sigma^2}\right)^5 \ ; \qquad \left(\frac{\delta p_t}{\delta t}\right)_{\rm bin3} = \left(\frac{\delta p_r}{\delta t}\right)_{\rm bin3} \tag{27}$$

Here a simple estimate using gravitational focusing and the probability that three particles come together have been employed. C_b is a constant of proportionality which ies expected to have a value between 75 and 90 for an equal mass system; for more details see the above cited papers.

2.2.3 The "Right Hand Sides"

All right hand sides of the moment equations 22–24 are calculated by multiplying the right hand side (the encounter term) of the Fokker-Planck equation as it occurs in Eq. 8 with the appropriate powers of u, v and w and integrating over velocity space. There is only one non-trivial encounter term to be determined for the collisional decay of anisotropy. It is self-consistently computed by assuming a certain Legendre series evaluation for f up to second order (i.e. including anisotropy) in the Appendix of [26], the result being ($p_a = p_r - p_t$):

$$\left(\frac{\delta p_a}{\delta t}\right)_{\rm enc} = -\frac{p_a}{t_a} \quad ; \quad t_a = \frac{10}{9} t_{\rm rx} \quad ; \quad t_{\rm rx} = \frac{9}{16\sqrt{\pi}} \frac{\sigma^3}{G^2 m \rho \ln(\gamma N)} \ . \tag{28}$$

t_a defined in the above equation denotes the characteristic decay time of anisotropy; $t_{\rm rx}$ is equivalent to the standard two–body relaxation time. The particular factors applied to it originate unambigously from the Fokker-Planck collisional term evaluation with the assumption of a certain normalization and functional form of f by a Legendre series. The procedure can be thoroughly followed in [49]. For the above result terms quadratic in p_a have been omitted. Comparisons with direct N-body simulations suggest a more general ansatz

$$\left(\frac{\delta p_a}{\delta t}\right)_{\rm enc} = -\frac{p_a}{\lambda_a t_a} \tag{29}$$

and it is shown that $\lambda_a = 0.1$ provides the best results [26]. Sect. 4 describes some examples how well the gaseous and Fokker-Planck models describe a star cluster's evolution as compared to a direct N-body simulation. There is no other way to check the theoretical models on the Fokker-Planck equation, because the timescale for exponential instability and deterministic chaos to occur in a self-gravitating star cluster consisting of many stars of equal or at least similar mass is of the same order as a crossing time [28]. There is no analytical or semianalytical general solution of the N-body problem available in that case for the unperturbed problem. In contrast to this in the case of solar system studies there is a semianalytic secular theory [50]) to be compared with the direct orbit integrations (see e.g. [51]). Here, for the star cluster case, we only can rely on the comparison of the numerical solutions obtained from different physical models, as there are direct N-body integrations and models based on the Fokker-Planck approximation.

3 Direct N-body Simulations – Methods and Algorithms

3.1 Introduction – Density and Potential Computation

To integrate the orbits of particles in time under their mutual gravitational interaction the total gravitational potential at each particle's position is required. Poisson's equation in integral form gives the potential Φ generated at a point in coordinate space $\vec{r}$ due to a smooth mass distribution $\rho(\vec{r})$

$$\Phi(\vec{r}) = -G \int \frac{\rho(\vec{r}')}{|\vec{r}' - \vec{r}|} d^3\vec{r}' \quad . \tag{30}$$

There are two fundamentally different methods to define the density distribution as a function of a given particle distribution. The first is based on a mesh in coordinate space; particles are sampled on the mesh and their mass divided by the cell volume, which provides a local density. This method called particle-mesh requires for good statistics a sufficient number of particles in each cell. There is no or very little intrinsic particle-particle relaxation with this method, but there is relaxation of particle energies due to the finite resolution of the mesh (see [38], and for a more recent cosmological application compare [44] and references therein). Refinements, by which particles are smeared out by low-order interpolation formulae (e.g. cloud-in-cell, CIC) or the acceleration is interpolated within the cells (e.g. Superbox [20]) are possible and reduce mesh relaxation.

The second method is based on the particles itself. A kernel function $W(\vec{x}, h)$ is defined, normalized by $\int W d^3\vec{x} = 1$, where h describes a typical length scale over which the influence of a particle decays. Therewith a sampled density ρ_s is defined in a mesh-free way as

$$\rho_s(\vec{r}) = \int W(\vec{r} - \vec{r}', h)\rho(\vec{r}')d^3\vec{r}' \tag{31}$$

where h is a characteristic smoothing length. A discrete particle distribution is given by $\rho(\vec{r}) = \sum \delta(\vec{r} - \vec{r}_j)$ with N particles distributed at positions $\vec{r}_j$. Hence we get a sampled density from the discrete particle distribution as

$$\rho_s(\vec{r}) = \sum_{j=1}^{N} m_j W(\vec{r} - \vec{r}', h) \tag{32}$$

As an estimate for the density and other thermodynamic quantities this method is used by "smoothed particle hydrodynamics" simulations [71], using kernel functions W with compact support, which means they are non-zero only in a bounded volume. Here, it is not intended to explain this further, the reader is referred to the literature and other papers of this volume. If one takes a δ-function for the kernel as well and puts this into the integral Poisson equation (30) Newton's law turns out again:

$$\Phi(\vec{r}) = -G \sum_{j=1}^{N} \frac{m_j}{|\vec{r} - \vec{r}_j|} \tag{33}$$

Certainly this could have been written down immediately, but the above description makes it easier to understand the relation of the direct potential summation to the other methods. In the following, the prototype N-body integration method using the above "brute-force" method, in a specific form called the Hermite scheme [60], shall be described in some more detail. It is the most commonly used method in the field of globular cluster dynamics and other studies requiring very high accuracies.

3.2 The Hermite Scheme

Assume a set of N particles with positions $\vec{r}_i(t_0)$ and velocities $\vec{v}_i(t_0)$ $(i = 1, \ldots, N)$ is given at time $t = t_0$, and let us look at a selected test particle at $\vec{r} = \vec{r}_0 = \vec{r}(t_0)$ and $\vec{v} = \vec{v}_0 = \vec{v}(t_0)$. Note that here and in the following the index i for the test particle i and also occasionally the index 0 indicating the time t_0 will be dropped for brevity; sums over j are to be understood to include all j with $j \neq i$, since there should be no self-interaction. Accelerations $\vec{a}_0$ and their time derivatives $\dot{\mathbf{a}}_0$ are calculated explicitly:

$$\vec{a}_0 = \sum_j G m_j \frac{\vec{R}_j}{R_j^3} \quad ; \quad \dot{\vec{a}}_0 = \sum_j G m_j \left[\frac{\vec{V}_j}{R_j^3} - \frac{3(\vec{V}_j \cdot \vec{R}_j)\vec{R}_j}{R_j^5} \right] , \tag{34}$$

where $\vec{R}_j := \vec{r} - \vec{r}_j$, $\vec{V}_j := \vec{v} - \vec{v}_j$, $R_j := |\vec{R}_j|$, $V_j := |\vec{V}_j|$. By low order predictions,

$$\vec{x}_p(t) = \frac{1}{6}(t - t_0)^3 \dot{\vec{a}}_0 + \frac{1}{2}(t - t_0)^2 \vec{a}_0 + (t - t_0)\vec{v} + \vec{x} \ , \tag{35}$$

$$\vec{v}_p(t) = \frac{1}{2}(t - t_0)^2 \dot{\vec{a}}_0 + (t - t_0)\vec{a}_0 + \vec{v} \ , \tag{36}$$

new positions and velocities for all particles at $t > t_0$ are calculated and used to determine a new acceleration and its derivative directly according to Eq. 34 at $t = t_1$, denoted by $\vec{a}_1$ and $\dot{\vec{a}}_1$. On the other hand $\vec{a}_1$ and $\dot{\vec{a}}_1$ can also be obtained from a Taylor series using higher derivatives of $\vec{a}$ at $t = t_0$:

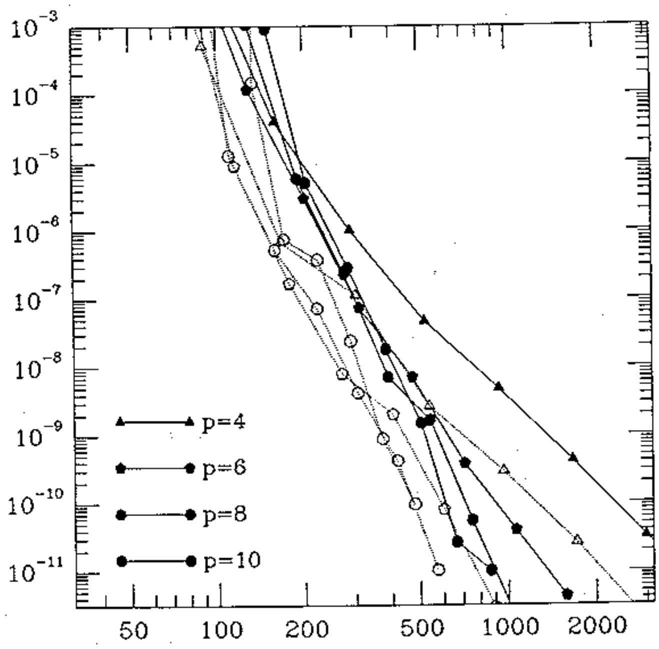

Fig. 1. The relative energy error as the function of the number of steps. A time-step criterion using differences between predicted and corrected values is used, different from Eq. 43. Dotted curves are for Hermite schemes, solid curves for Aarseth schemes. The stepnumber p denotes the order of the integrator. From [57].

$$\vec{a}_1 = \frac{1}{6}(t-t_0)^3\vec{a}_0^{(3)} + \frac{1}{2}(t-t_0)^2\vec{a}_0^{(2)} + (t-t_0)\dot{\vec{a}}_0 + \vec{a}_0 \ , \tag{37}$$

$$\dot{\vec{a}}_1 = \frac{1}{2}(t-t_0)^2\vec{a}_0^{(3)} + (t-t_0)\vec{a}_0^{(2)} + \dot{\vec{a}}_0 \ . \tag{38}$$

If $\vec{a}_1$ and $\dot{\vec{a}}_1$ is known from direct summation (from Eq. 34 using the predicted positions and velocities) one can invert the equations above to determine the unknown higher order derivatives of the acceleration at $t = t_0$ for the test particle:

$$\frac{1}{2}\vec{a}^{(2)} = -3\frac{\vec{a}_0 - \vec{a}_1}{(t-t_0)^2} - \frac{2\dot{\vec{a}}_0 + \dot{\vec{a}}_1}{(t-t_0)} \tag{39}$$

$$\frac{1}{6}\vec{a}^{(3)} = 2\frac{\vec{a}_0 - \vec{a}_1}{(t-t_0)^3} - \frac{\dot{\vec{a}}_0 + \dot{\vec{a}}_1}{(t-t_0)^2} \ , \tag{40}$$

This is the Hermite interpolation, which finally allows to correct positions and velocities at t_1 to high order from

$$\vec{x}(t) = \vec{x}_p(t) + \frac{1}{24}(t-t_0)^4\vec{a}_0^{(2)} + \frac{1}{120}(t-t_0)^5\vec{a}^{(3)} \ , \tag{41}$$

$$\vec{v}(t) = \vec{v}_p(t) + \frac{1}{6}(t-t_0)^3\vec{a}_0^{(2)} + \frac{1}{24}(t-t_0)^4\vec{a}_0^{(3)} \ . \tag{42}$$

Taking the time derivative of Eq. 42 it turns out that the error in the force calculation for this method is $\mathcal{O}(\Delta t^4)$, as opposed to the widely used leap-frog schemes, which have a force error of $\mathcal{O}(\Delta t^2)$. Additional errors induced by approximate potential calculations (particle mesh or TREE) create potentially even larger errors than that. In Fig. 1, however, it is shown that the above Hermite method used for a real N-body integration sustains an error of $\mathcal{O}(\Delta t^4)$ for the entire calculation. Many persons in the world know as Aarseth scheme (in particular the code version NBODY5 [1]) an integrator of the same order as the Hermite scheme, but using only accelerations on four time points instead of $\vec{a}$ and $\dot{\vec{a}}$ on two time points. As is shown in [57], the Aarseth scheme is $\mathcal{O}(\Delta t^4)$ as well, but for the same number of time steps the absolute value of the energy error (not its slope) is clearly smaller in the Hermite scheme. This means that for a given energy error the Hermite scheme allows timesteps which are larger by some factor of order unity depending on the parameters of the system under study. The Hermite scheme has been commonly adopted during the past years, because it needs less memory, and allows slightly larger timesteps. More importantly, after the addition of a hierarchical (as opposed to individual) time step scheme it is well suited for parallelization on modern special and general purpose high performance computers [81]. The timestep scheme will be discussed now.

3.3 Choice of Timesteps – Parallelization

[1] provides an empirical timestep criterion

$$\Delta t = \sqrt{\eta \frac{|\vec{a}||\vec{a}^{(2)}| + |\dot{\vec{a}}|^2}{|\dot{\vec{a}}||\vec{a}^{(3)}| + |\vec{a}^{(2)}|^2}} \ . \tag{43}$$

The error is governed by the choice of η, which in most practical applications is taken to be $\eta = 0.01 - 0.04$. It is instructive to compare this with the inverse square of the curvature κ of the curve $\vec{a}(t)$ in coordinate space

$$\frac{1}{\kappa^2} = \frac{1 + |\dot{\vec{a}}|^2}{|\vec{a}^{(2)}|^2} \ . \tag{44}$$

Clearly under certain conditions the time step choice Eq. 43 becomes similar to choosing the timestep according to the curvature of the acceleration curve; since it was determined just empirically, however, it cannot generally be related to the curvature expression above. In [57] a different time step criterion has been suggested, which appears simpler and more straightforwardly defined, and couples the timestep to the difference between predicted and corrected

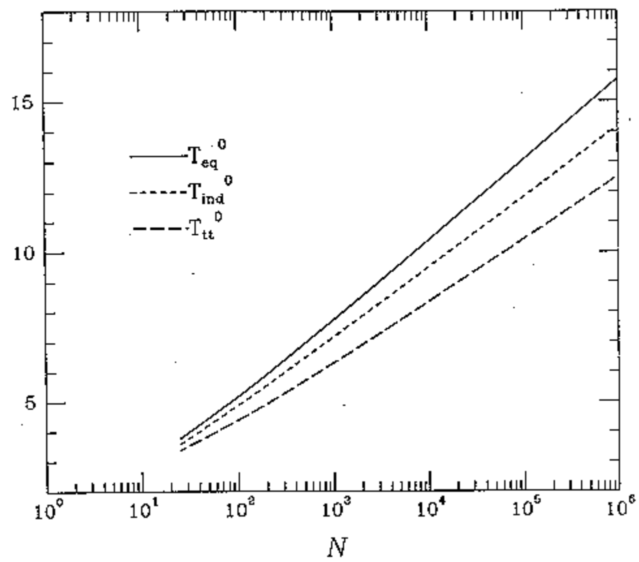

Fig. 2. The logarithm of T, the total computing time required to advance the N-body system for one crossing time plotted as a function of the particle number N for the equal time step scheme $T_{\rm eq}$, the individual time step scheme $T_{\rm ind}$ and the Ahmad-Cohen neighour scheme with two levels of individual time steps $T_{\rm tt}$. The unit of computing time is the time required to calculate the force between a pair of particles. The system is assumed to be homogeneous. From [61].

coordinates. The standard Aarseth time step criterion Eq. 43 has been used in most N-body simulations so far (but compare the discussion in [84]).

Since the position of all field particles can be determined at any time by the low-order prediction Eq. 36, the time step of each particle (which determines the time at which the corrector Eq. 42 is applied) can be freely chosen according to the local requirements of the test particle; the additional error induced due to the use of only predicted data for the full N sums of Eq. 34 is negligibly small, for the benefit of not being forced to keep all particles in lockstep. Such an individual time step scheme is in particular for non-homogeneous systems very advantageous, as was quantitatively pointed out by [61]. Particles in the high density core of a star clusters need to be updated much more often than particles on orbits very far from the centre. They show that the gain in computational speed due to the individual time step scheme (as compared to a lockstep scheme where all particles share the minimum required time step) is of the order $N^{1/3}$ for homogeneous and N^1 for strongly spatially structured systems; we show their results as Figs. 2, 3.

For the purpose of vectorization and parallelization it is better not to have the particles continuously distributed on a time axis. Consequently, [58] uses a hierarchical scheme, still on the basis of Eq. 43; but a change of the timestep is considered only if that equation yields a variation of Δt compared to the last step by more than a factor of 2 (increase or decrease). If this is the case a variation by 2 is applied only. Thus in model units all timesteps are selected from the set $\{2^{-i}|i = 0, ...i_{\rm max}\}$ with $k = i_{\rm max}$ determined by the

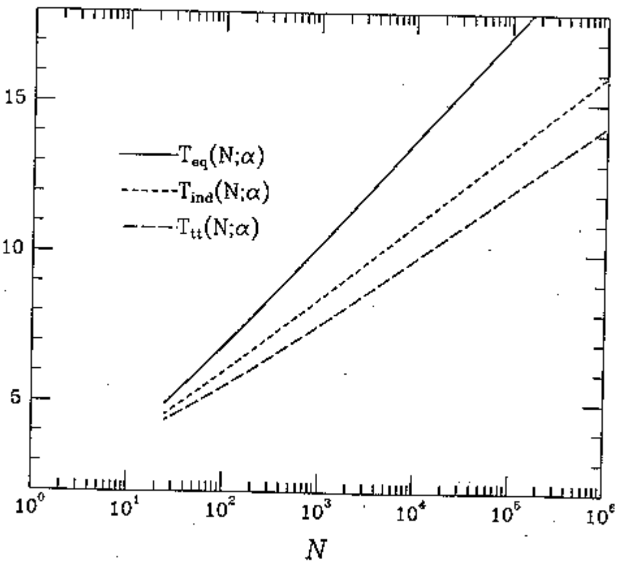

Fig. 3. As Fig. 2, but for the system with a power-law density distribution $\rho \propto r^{-2.25}$. From [61].

condition that $\Delta t_{\min} > 2^{-i_{\max}}$ for the minimum timestep $\Delta t_{\min}$ determined from Eq. 43. For core collapse simulations of star clusters of a few ten thousand particles $i_{\max}$ goes up to about 20; empirically and theoretically [61] $\Delta t_{\min} \propto N^{-1/3}$, so for large N $i_{\max}$ becomes larger, however, on the other hand, how large $i_{\max}$ grows for fixed N depends on the selected criteria for so–called KS regularisation of perturbed two–body motion (see below). The implementation of the block step scheme indeed uses an even stronger condition than the above described one, it is demanded that not only the time steps, but also the individual accumulated times of each particles are commensurate with the timestep itself. This ensures that for any particle i and any time $T_i = t_i + \delta t_i$ *all* particles with $\delta t_j < \delta t_i$ have for their own time $T_j = t_j + \delta t_j = T_i$, where the last equality is the non–trivial one. Such procedure is important for the parallelization of the algorithm. For example it has as a consequence that at the big time steps always huge groups of particles are due for correction, sometimes even all particles (at the largest steps). Such scheme allows an efficient parallelization of all operations necessary for calculation of $\vec{a}$ and $\dot{\vec{a}}$ and for the update of particle positions and velocities (corrections). Special purpose computers have been built tailored to the Hermite codes, which are denoted as HARP ("Hermite Accelerator Pipeline") boards and stem from the bigger GRAPE–family [83,63]. Such HARP–boards have been made available also at some places outside Japan, including "Astronomisches Rechen–Institut" Heidelberg (for an application see e.g. [88]).

Another refinement of the Hermite or Aarseth "brute force" method is the two-time step scheme, denoted as neighbour or Ahmad-Cohen scheme [5]. For each particle a neighbour radius is defined, and $\vec{a}$ and $\dot{\vec{a}}$ are computed due to neighbours and non-neighbours separately. Similar to the Hermite scheme the higher derivatives are computed separately for the neighbour force (irregular

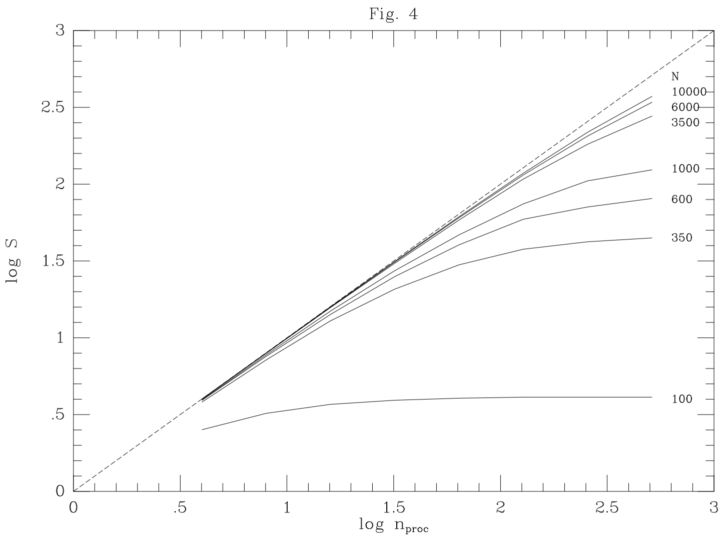

Fig. 4. Theoretical speedup (neglecting communication) of regular force calculation as a function of processor number for varying particle number N. The dashed line is the ideal maximum speed up which could be reached on a given processor number.

force) and non-neighbour force (regular force). Computing two timesteps, an irregular small $\Delta t_{\rm irr}$ and a regular large $\Delta t_{\rm reg}$, from these two force components by Eq. 43 yields a timestep ratio of $\gamma := \Delta t_{\rm reg}/\Delta t_{\rm irr}$ being in a typical range of 5–20 for N of the order 10^3 to 10^4. The reason is that the regular force has much less fluctuations than the irregular force. The Ahmad-Cohen neighbour scheme is implemented in a self-regulated way, where at each regular time-step a new neighbour list is determined using a given neighbour radius r_{si} for each particle. If the neighbour number found is larger than the prescribed optimal neighbour number, the neighbour radius is increased or vice versa. In [1,61] more complicated algorithms to adjust the neighbour radius are described. On the contrary to [61], who find an optimal neighbour number of $N_{n,\rm opt} \propto N^{3/4}$ we find that adopting a constant neighbour number of the order of $20 - 50$ is sufficient at least up to $N = 50000$. The reason is that by using special purpose machines or parallelization for parts of the code, an optimal neighbour number is not well defined, so the neighbour number can be selected according to accuracy and efficiency requirements [81]. After each regular time step the new neighbour list is communicated along with the new particle positions to all processors of the parallel machine, thus making it possible to do the irregular time step in parallel as well.

Using a two-time step or neighbour scheme again increases the computational speed of the entire integration by a factor of at least proportional to $N^{1/4}$ [57]. Both the regular and irregular timesteps are arranged in the hierarchical, commensurable way, and the total inherent parallelism in the resulting algorithm is depicted in Figs. 4, 5 from [81] for the irregular and the regular step. One can see that even for moderate particle numbers of 10^4 particles some 512 processors could be used efficiently. Sometimes there are only very

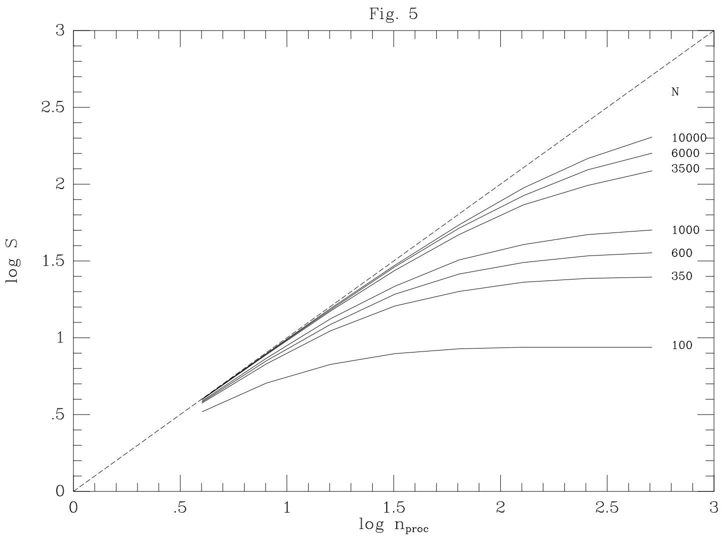

Fig. 5. As Fig. 4, for the irregular (neigbour) force calculation.

few particles in the smallest steps to be integrated, which one might consider as being very prohibitive for parallelization. However, due to the large number of medium and large size blocks this effect is negligible for the overall performance. It causes however, the saturation in the curves in Figs. 4 and 5 which defines the limit for the number of processors useful for a given particle number N. By using more and more processors in the parallel execution one finds that the asymptotic scaling of the "brute force" N-body problem can be reduced effectively to an N scaling (Fig. 6). But in our present implementation the parallelization is done only according to parallel sections (do loops) in the code; there is no domain decomposition (distributing particles on the processor). Thus at the end of any timesteps new results have to be broadcast to all other processing units. A systolic algorithm is used for that which scales linearly in communication time with the number of processors. It is interesting to note an approach suggested by molecular dynamicists to use a new kind of hyper-systolic communication algorithm, which scales only by the square root of the processor number [52,53]. Presently we think that hyper-systolic algorithms can efficiently be used only if the sum over all particles for the acceleration and its time derivative (Eq. 34) should be directly parallelized. The number of interprocessor communications $N_{\rm comm}$ for the hyper-systolic algorithm is of the order $N\sqrt{n_{\rm PE}}$; on the other hand our algorithm, which we would like to call here "parallel group execution algorithm" [81], has a scaling $N_{\rm comm} \propto N^{2/3} n_{\rm PE}$, because only subgroups of particles, whose size scales with $N^{2/3}$ have to be communicated across the processor network. In other words, asymptotically (above some critical particle number as a function of $n_{\rm PE}$, the hyper-systolic algorithm should lose against the parallel group execution algorithm. However, these questions have not yet been examined in detail, for example what the critical N really are and which algorithm is more efficient for practically useful particle numbers of today. This is subject of present and future work.

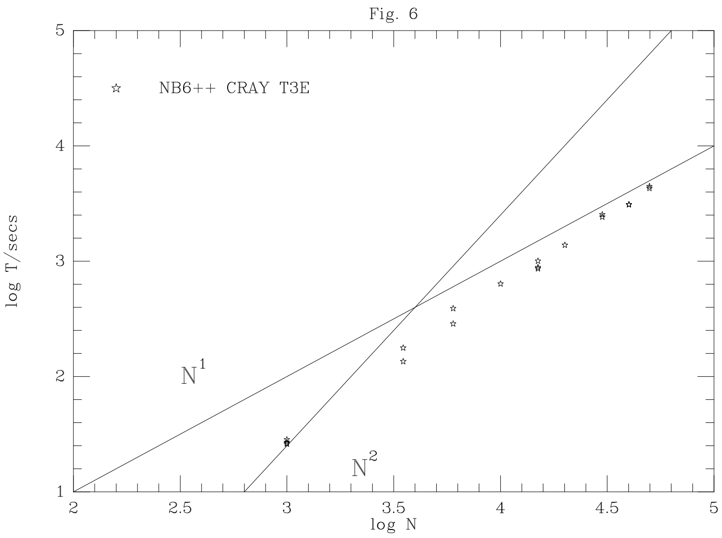

Fig. 6. CPU time needed for one N-body time unit as a function of particle number N using NBODY6++ on the CRAY T3E. The collection of data points includes runs with varying average neighbour number and processor/pipeline number, starting from 8 for low N up to 512 for the largest N, which are not individually discriminated in the figure.

If the two-body force between any pair of particles becomes dominant their (perturbed) relative motion is integrated in special regularized coordinates (taking into account perturbations from field particles), in which the singularity of the two-body motion is transformed into a slowly varying parameter (the binding energy) and does not occur in the integration variables. The rest of the N-body simulation generally regards the regularized pair as a compound particle located at the position and moving with the velocity of its centre of mass, except in the case when a perturber moves very close to a regularized pair (in such cases the pair is resolved). It was already discovered in the earliest published N-body simulations that the formation of close and eccentric binaries occurs as the rule rather than as an exception and that it was particularly difficult to accurately integrate them [39,40]. As a consequence two-body, three-body and chain regularizations were developed and implemented in order to accurately and efficiently integrate star clusters including all their close binaries, triples and hierarchical subsystems. An excellent account of regularization, historically and scientifically, can be found in [66]. Most recent developments are the slow-down treatment of tight binaries [67] and a new method to gain accuracy and exact solutions in the unperturbed case using Stumpff functions [68].

Recently the necessity of regularization was challenged and its replacement by a binary tree structure for hierarchical systems with relative coordinates has been suggested [62]. However, the regularisation procedure is undisputedly much more efficient and accurate for highly eccentric binaries, and the new method has not yet been widely applied and proven to work through the most delicate phase of core bounce and post-collapse evolution in point-mass systems or systems with many primordial hard binaries.

3.4 Exponential Instability, Validity of N-body simulations, Planetary System Integrations

Concerning the algorithms explained in the previous paragraph the direct N-body simulation may turn out to be the most reliable (although computationally most expensive) way to simulate the dynamical evolution of a gravitating system consisting of N point masses. It does not involve any serious approximations and assumptions, as e.g. the Fokker-Planck approximation in the gaseous models. By reducing the η-values any accuracy can be achieved in principle, as far as the globally conserved quantities (energy, angular momentum) are concerned. However, for a system with N particles phase space has $6N$ dimensions, and a check of say energy and angular momentum alone only checks whether the numerically calculated system remains within the allowed $6N - 4$ dimensional hypervolume. There is no a priori information how "exact" the individual trajectories are reproduced in the simulation. [69] pointed out that, due to repeated close encounters occurring between particles initial configurations that are very close to each other, quickly diverge in their evolution from each other. He could show that the separation in phase space of two trajectories increases exponentially with time, or with other words, the evolution of the configuration is extremely sensitive to initial conditions (particle positions and velocities). The timescale of exponential instability is as short as a fraction of a crossing time, and the accurate integration of a system to core collapse would require of order $\mathcal{O}(N)$ decimal places [28,45]. Those papers argue that the problem is caused by two-body encounters, but chaotic orbits in non-integrable potentials can be a source of exponential instability and thus cause unreliable numerical integrations as well.

However, the situation is not as bad as it seems. N-body simulations for star clusters or galactic nuclei do not really exploit the detailed configuration space of all particles. Quantities of interest are global or somehow averaged quantities, like Lagrangian radii or velocity dispersions averaged in certain volumes. As it was nicely demonstrated in the pioneering series of papers by [22–25] such results are not sensitive to small variations of initial parameters. They took statistically independent initial models (positions and velocities at the beginning selected by different random number sets) and showed that the ensemble average of the dynamical evolution of the system always evolved predictably and in remarkable accord with results obtained from the Fokker-Planck approximation. The method was also partly and successfully used in [26], which focused on the evolution of anisotropy and comparisons with the anisotropic gaseous models of the author of this paper.

As a consequence, it should be remembered, however, that great care has to be taken when interpreting results of N-body simulations on a particle by particle basis, for example determining rates of specific types of encounters, which could produce mergers in a large direct N-body model.

The long-term behaviour of dynamical systems as the solar system are being studied by N-body simulations as well, but clearly there are much higher requirements on the accuracy of the individual orbits in contrast to the star cluster problem. Therefore for the solar system dynamics symplectic methods, using a generalized leap-frog, like the widely used Wisdom-Holman symplectic mapping method [89] are the standard integration method. As a non-exhaustive reference the reader might look into a recent study of the relation between the earth-moon system and the stability of the inner solar system using this method [43] and a contemporary review [16]. Symplectic mapping methods do not show secular errors in energy and angular momentum. However, in their standard implementation they require a constant timestep. A generalization using a time transformation simultaneously with the generalized leap-frog has been suggested which can cope with variable timesteps [65]. Another more practical approach to strongly reduce secular errors is to enforce a time-symmetric scheme by making the timesteps reversible through an iteration [42,21]. How well this generally works and its relation to symplectic schemes is presently not clear. In [68] it is stressed that even with a newly applied classical method secular errors in the integration of close binaries can be strongly reduced. One should keep in mind though, that the N-body integration schemes discussed in this paper yield excellent results in the star cluster research (see Sect. 4) but are unsuitable for long-term solar system studies, because they generally have secular errors, although small. As outlined above in star cluster simulations the secular errors are being kept small relative to typical values of energy and angular momentum and an accurate reproduction of all individual stellar orbits is not generally required.

3.5 What about TREE- *and fast multipole codes?*

Finally, remarks shall be made on two very widely used algorithms to compute gravitational potentials from particle distributions namely the TREE- and fast multipole (FMP) algorithms. The TREE- method of [6] divides the system into hierarchical cells. The mutual interaction between particles or cells is resolved only if the opening parameter $\theta = r/d$, where r is the distance to and d a size scale of the cell under consideration, is smaller than a prescribed critical $\theta_{\rm crit}$. If the cell is not resolved because $\theta < \theta_{\rm crit}$, there is still the option to evaluate multipole moments of its internal mass distribution for the interaction with external particles. As one can see from Fig. 7, a global accuracy requirement of $\Delta E/E \approx 10^{-5}$ demands $\theta_{\rm crit} \approx 0.2$, a value much smaller than the usually effi-

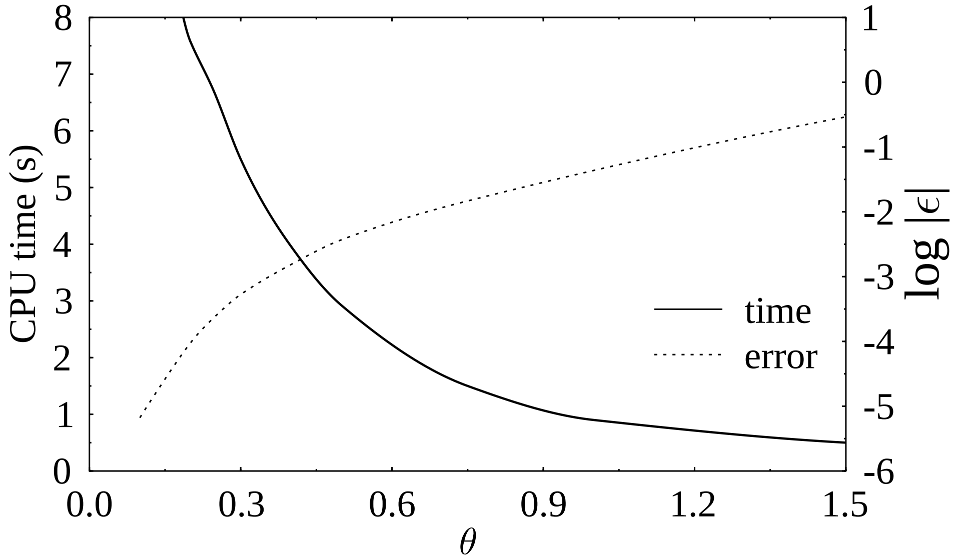

Fig. 7. Tradeoff between CPU time per step and average force error for the TREE-code with monopole terms only. From Fig. 4.11. of [74].

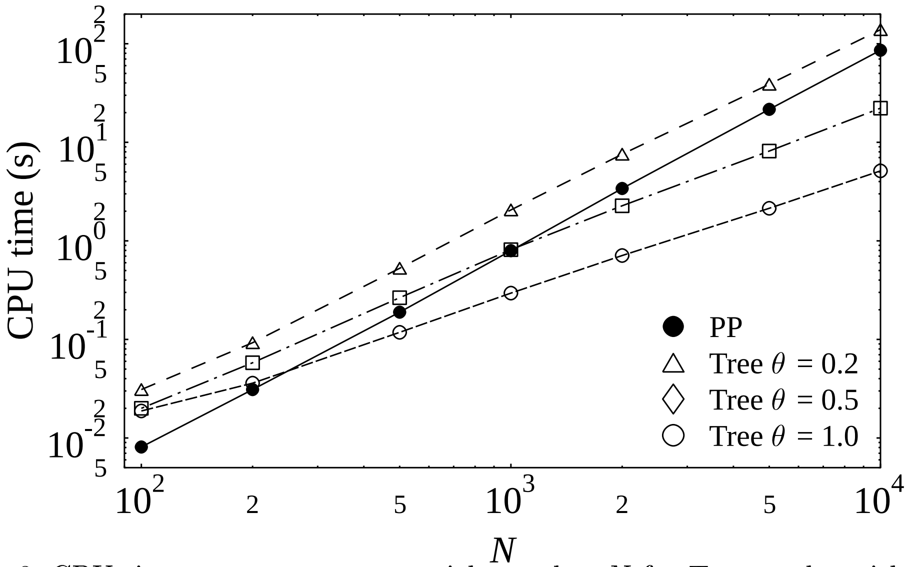

Fig. 8. CPU time per step versus particle number N for TREE-codes with varying opening parameter θ and a direct full "brute-force" labelled with PP in the figure (for "particle–particle"). From Fig. 4.9. of [74].

cient choice of 0.5–0.7, at which the computational time scales approximately as $\mathcal{O}(N \ln N)$. Looking then at Fig. 8, the computational time for the TREE-code with $\theta_{\rm crit} \approx 0.2$ scales nearly as $\mathcal{O}(N^2)$, i.e. like a "brute force" algorithm. So for each particle number and required accuracy one should carefully check whether a TREE-code or a direct N-body code are the best choice.

Another TREE-based algorithm is the fast-multipole method (FMT) proposed by [30,31]. The pair-wise potential in Eq. 30 is approximated by a multipole series, which can be done for arbitrary precision if enough terms are included. The multipole terms used for different test particles can be transformed into each other by using clever addition theorems for spherical harmonics, so the

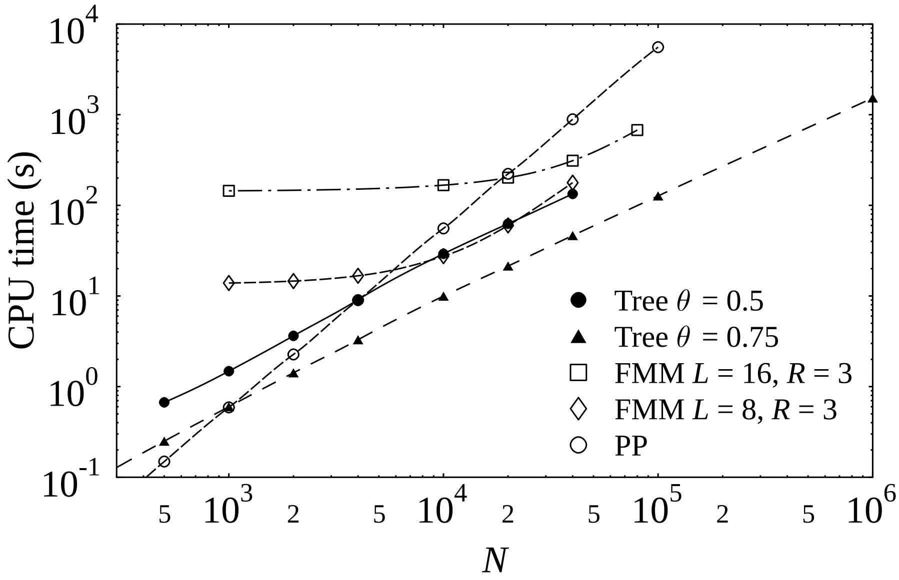

Fig. 9. Comparison of computational time as a function of particle number N between particle-particle, hierarchical TREE, and the fast multipole code. From Fig. 7.14 of [74].

entire algorithm scales in its computational demand with $\mathcal{O}(N)$ only. Higher precision only changes the proportionality factor, not the scaling (as in the case of the TREE-code, which effectively becomes a "brute force" code if high enough accuracy is demanded. However, such a code is fine only for homogeneous or nearly homogeneous systems, as they occur in plasma physics. In all cases where there is strong spatial structure, like in astrophysical star clusters, [61] have demonstrated that the use of an individual time step scheme in an $\mathcal{O}(N^2)$ code gains a factor at least $\propto N$ in efficiency. So, asymptotically a "brute-force" integrator with individual timesteps is more efficient than an FMT integrator. The latter is based on an equal timestep for all particles (otherwise it would lose its $\mathcal{O}(N)$ property; so both codes have asymptotically the same N scaling, but then the overhead (proportionality) factor is much smaller in the direct force summation than in the multipole evaluation. This can be seen also from Fig. 9 in [74] for low N. For the direct calculation method in this plot, the individual time step scheme is not taken into account.

The information contained in the previous paragraphs, complemented by some additional details and references, which will not be elaborated in more detail here, are presented in an overview in Table 1. It is divided into three boxes, the first for the mesh or series evaluation codes, which do not contain particle-particle forces and thus are not appropriate for direct modelling of relaxing systems. The second box contains the classical direct "brute force" N-body codes, whereas the third one contains algorithms which cannot clearly be counted to one of the other two groups.

Table 1

Algorithms for N-body Simulations
N: particle, N_n: characteristic neighbour number
n_c: number of grid cells in one dimension, nlm: order in 3D series evaluation

Acronym	Algorithm	Scaling	Comments
PM	Particle Mesh	$N\ n_c^3 \log_2 n_c^3$ (1)	fixed geometry
FMP	Fast Multipole	$N\ nlm$	req. equal Δt
SCF	Self-Consistent Field	$N\ nlm$	series evaluation (2)
NBODY1	Aarseth	N^2	ITS, softening
NBODY1++	Hermite	N^2	HTS, softening
NBODY2	Aarseth, AC	$NN_n + N^2/\gamma$	ITS, softening, (3)
NBODY3	Aarseth	N^2	ITS, KS-reg.
NBODY4	Hermite	N^2	HTS, KS-reg.
NBODY5	Aarseth, AC	$NN_n + N^2/\gamma$	ITS, KS-reg., (3)
NBODY6	Hermite, AC	$NN_n + N^2/\gamma$	HTS, KS-reg., (3)
NBODY6++	parallel NBODY6	$NN_n + N^2/\gamma$	HTS, KS-reg., (3,4)
KIRA	Hermite	N^2	HTS, (5)
TREE	TREE-code	$N \ln N$	N^2 for high accuracy
P^{3}M	Part.-Part. PM	$N_n^2\ n_c^3 \log_2 n_c^3$ (1)	fixed geometry (6)

softening: singularity in pairwise potential removed by softening parameter ε
ITS: Individual Time Step Scheme
HTS: Hierarchical Block Time Step Scheme
KS-reg.: KS regularization of perturbed two- and hierarchical N-body motion [48,68]
AC: Ahmad-Cohen neighbour scheme [5]
(1) Discrete FFT on regular 3D mesh with n linear mesh points assumed
(2) Sufficient Accuracy requires appropriate basis function set [37]
(3) γ: ratio of regular to irregular time step
(4) speedup by parallel execution not contained in scaling, see [81]
(5) New high accuracy Hermite code based on STARLAB [64,75]
(6) with hierarchically nested adaptive grids used for cosmological simulations [73]

4 Application to Star Clusters

Since this article is focused on the physical and numerical methods of calculating the evolution of relaxing star clusters, only a brief account of some of the physical problems and challenges will be given here, which have been and will be tackled by the previously described models. Despite of a wealth of beautiful observational data provided by e.g. Hubble space telescope observations of globular clusters some of the fundamental questions related to the validity

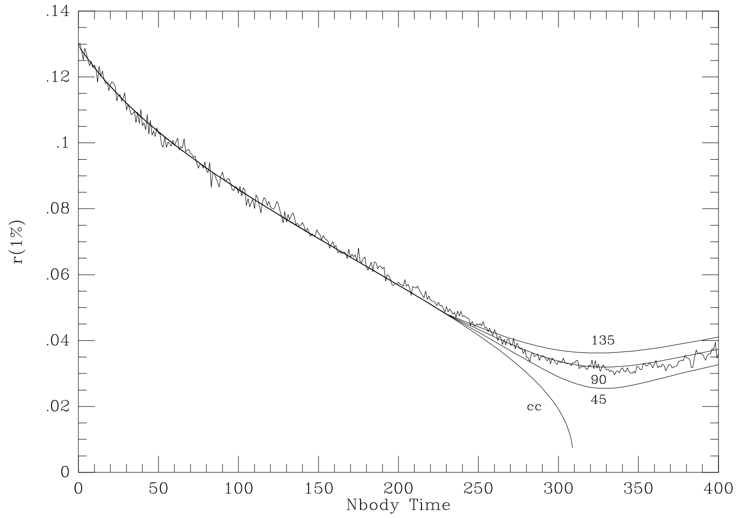

Fig. 10. Evolution of the 1% Lagrangian radius in the averaged $N = 1000$ N-body model in comparison to the anisotropic gaseous model for different strength of the binary energy generation parameter C_b (see Eq. 27). The subscript cc indicates a pure core collapse gaseous model without binary heating.

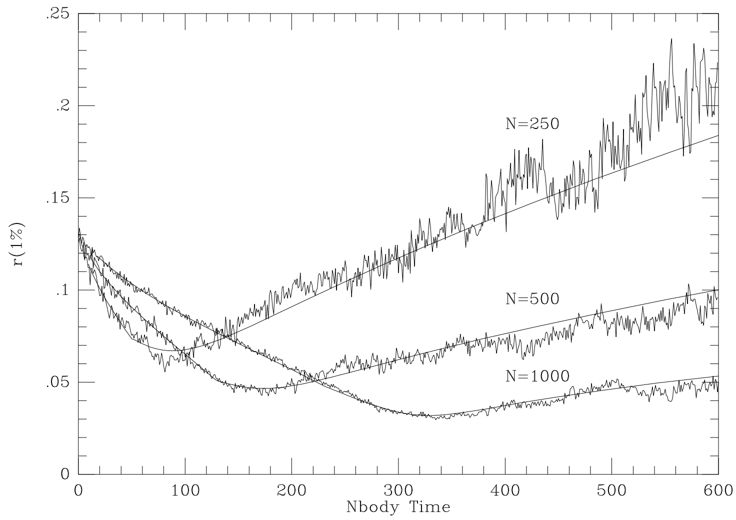

Fig. 11. Evolution of the 1% Lagrangian radius in the averaged 1000, 50, 250 body models in comparison to the anisotropic gaseous models using C_b = 90, 70, 55, respectively.

of the N-body approach and the other approximate models still deserve attention as they can lead to very fascinating general questions regarding the thermodynamical behaviour of large N-body systems.

A series of papers has been devoted to the comparison of ensemble averaged N-body simulations ($N \leq 2000$) with the expectations derived from Fokker-Planck or gaseous models [26,22–25]. Here we show as an example, in Figs. 10 and 11, the excellent agreement reached between the anisotropic gaseous model and the ensemble averaged N-body system. The models started with

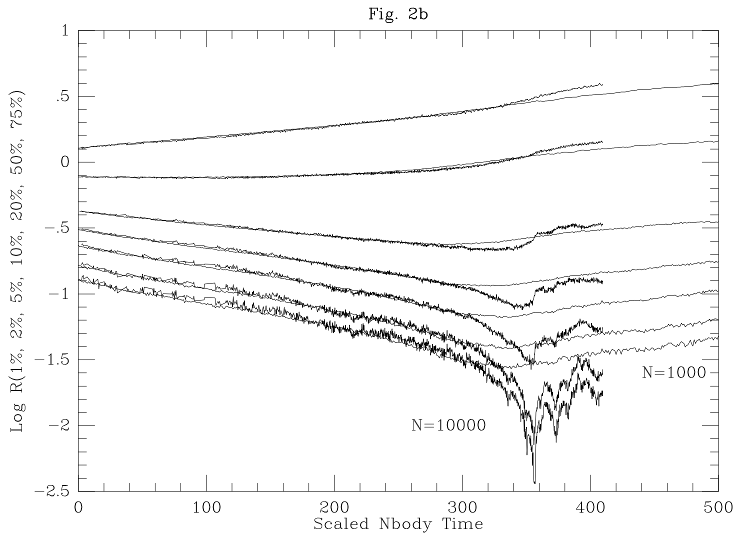

Fig. 12. Lagrangian radii containing the indicated fraction of total mass as a function of time for a single 10^4-body simulation (fluctuating curves) compared to an averaged $N = 1000$ simulation of [22,23]. Times scaled as explained in main text.

an initial Plummer model and follow the core collapse induced by heat conduction and the post-collapse evolution due to formation and hardening of three-body hard binaries. The agreement of both types of models mutually supports both sides: it shows that by ensemble averaging, the exponential instability of the N-body system does not spoil the physically correct behaviour of the system. It also demonstrates that the Fokker-Planck approximation, especially with its underlying assumption of strict spherical symmetry and dominance of small-angle two-body encounters for relaxation (i.e. neglectance of collective processes), is correct. It also shows that the very simple algorithm to describe the heating provided by the formation of close three-body binaries and their subsequent hardening by superelastic binary-single star encounters, which was first introduced into the gaseous models by [9], provides a surprisingly good description of the real processes in the average N-body system. The cited paper ignited a discussion over many years whether gravothermal oscillations, being a thermodynamic consequence of heat conduction by two–body relaxation, will prevail in a real N-body system with all its stochastic fluctuations. The question was settled after an N-body simulation on the massively parallel Teraflop GRAPE machine [63] using a high-accuracy Hermite scheme, as described above, became available. Gravothermal oscillations were found in a very large $N = 32000$ particle simulation [59].

In Fig. 12 we show a striking example of the validity of the Fokker-Planck approximation even for a single large direct N-body-simulation, here using NBODY5, an Aarseth scheme (see Table 1), for 10000 particles, a model simulation again starting with Plummer's model and undergoing core collapse and core bounce due to hard binaries [80]. The average $N = 1000$ particle model by [22] has been taken and its time was scaled with the factor $N/\ln(\gamma N)$, which

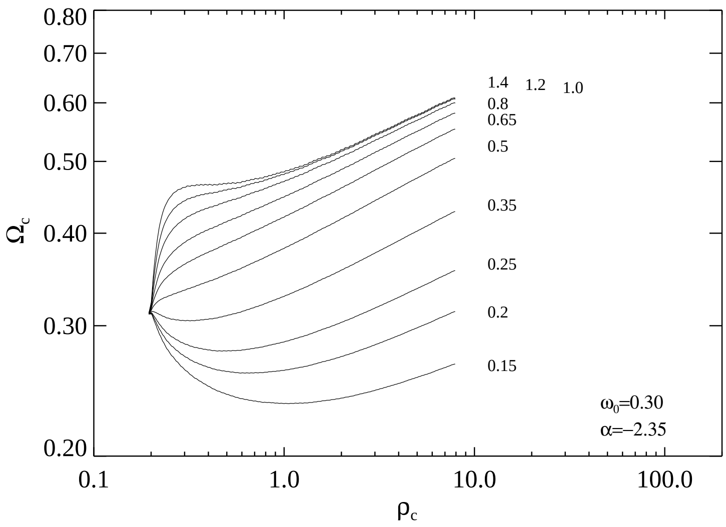

Fig. 13. Evolution of central angular velocities versus central density of all 10 mass bins used in the calculation for an initial model with dimensionless central potential $W_0 = 3$ and dimensionless angular velocity $\omega_0 = 0.30$. The highest mass bin with $m = 1.4\ M_\odot$ is the uppermost curve, while the lowest mass bin with $m = 0.15\ M_\odot$ is the lowest curve. The parameters W_0 and ω_0 refer to an initial Michie-King model.

is the scaling of the standard two–body relaxation time Eq. 4. An excellent match between the evolution of the Lagrangian radii for the two systems occurs after such scaling, proving that it is indeed the standard relaxation which dominates the pre-collapse evolution. The differences between the two systems show up at the moment of the formation of the first three-body binaries, after which one expects the evolution not to scale as the relaxation time. In simple terms, the larger N, the less important are three-body effects as compared to the global potential; hence for large particle numbers the system collapses to higher densities and three-body effects finally dominate because they depend on the third power of the particle density as compared to the n^2 dependence of two-body relaxation.

Finally, we show a result from [17] in Fig. 13, a new multi-mass model using the orbit averaged Fokker-Planck approximation for axisymmetric rotating relaxing star clusters. The standard effect of mass segregation of the heavy masses is accompanied here by an acceleration of their rotational speed as compared to the small masses. Such interesting dynamical behaviour occurs just due to point-mass relaxation processes starting with a very simple tidally truncated rotating King model without any mass or rotational segregation. It is a yet unpublished generalization of equal mass rotating star cluster models [18]. They neglect the possible dynamical effect of non-classical third integrals, since it is assumed that the distribution function depends on energy and z-component of the angular momentum only. Such approximation needs to be checked by direct N-body models, which is the subject of on-going work. The results will also be important for the dynamical study of rotating galactic nuclei containing massive star-accreting black holes.

The reader should be made aware of the problem of scaling in the description of escaping stars from globular clusters [75,3] being tackled by large direct N-body simulations and their comparisons with approximate models. There are more challenges, like the inclusion of many close binaries already originating from star formation processes (for a calculation using NBODY5 see [46], compare also [11,47] for the study of mass segregation in young forming star clusters by means of direct N-body models). Finite sizes of stars lead to merging in high-density phases and cause population gradients and unusually high frequencies of exotic objects like blue stragglers and pulsars in the cores and haloes of globular clusters. Attempts to model all these processes in direct N-body models, with as many ingredients and realistic features included as possible are under way [2]. Ultimately we will be able from such models to provide synthetic observational data as e.g. color-magnitude diagrams.

Acknowledgements

Part of the work presented here was supported by DFG grants Sp 345/3-3 and 5-3. Computational time on the CRAY T3E parallel machines at HLRZ Jülich and HLRS Stuttgart is gratefully acknowledged. I thank the “Grapeyard” in Tokyo (Jun Makino and all other colleagues) for the continuous support and cooperation in all aspects regarding the GRAPE hardware and its scientific use. I am very grateful to Sverre Aarseth, for teaching me the art of N-body simulations years ago and continuously supplying new pieces of code and ideas. This work would not have been possible without his support. Thanks go also to Sverre Aarseth, Hugh Couchman, and Pavel Kroupa for helpful comments and suggestions.

References

[1] Aarseth S.J., in Brackbill J,U., Cohen B.I., eds, Multiple time scales, Academic Press, Orlando (1985) 378

[2] Aarseth S.J., in Hut P., Makino J., eds, Dynamical Evolution of Star Clusters, Proc. IAU Symp. No. 174, Kluwer, Dordrecht (1996) 161 Dordrecht, p.

[3] Aarseth S.J., Heggie D.C., *Monthly Notices Roy. Astron. Soc.*, **297** (1998) 794

[4] Aarseth S.J., Hénon M., Wielen R., *Astron. Astrophys.*, **37** (1974) 183

[5] Ahmad A., Cohen L., *Journ. Comp. Phys.*, **12** (1973) 389

[6] Barnes J., Hut P., *Nature*, **324** (1986) 446

[7] Bettwieser E., *Monthly Notices Roy. Astron. Soc.*, **203** (1983) 811

[8] Bettwieser E., Spurzem R., *Astron. Astrophys.*, **161** (1986) 102

[9] Bettwieser E., Sugimoto D., *Monthly Notices Roy. Astron. Soc.*, **208** (1984) 439

[10] Binney J., Tremaine S., Galactic Dynamics, Princeton Series in Astrophysics, Princeton University Press, New Jersey, USA (1987)

[11] Bonnell I., Davies M.B., *Monthly Notices Roy. Astron. Soc.*, **295** (1998) 691

[12] Cohn H., *Astrophys. J.*, **242** (1980) 765

[13] Cohn H., Hut P., Wise M., *Astrophys. J.*, **342** (1989) 814

[14] Djorgovski S., Meylan G., *Astron. J.*, **108** (1994) 1292

[15] Drukier G., *Astrophys. J. Suppl.*, **100** (1995) 347

[16] Duncan M.J., Quinn T., *Ann. Rev. Astron. Astrophys.*, **31** (1993) 265

[17] Einsel C., in Duschl, W., Einsel C., eds, Dynamics of Galaxies and Galactic Nuclei, Proc. Ser. I.T.A., No. 2, Heidelberg (1998) in press

[18] Einsel C., Spurzem R., *Monthly Notices Roy. Astron. Soc.*, **302** (1999) 81

[19] Elson R., Hut P., Inagaki S., *Ann. Rev. Astron. Astrophys.*, **25** (1987) 565

[20] Fellhauer M., Kroupa P., Baumgardt H., Bien R., Spurzem R., Wassmer N., *Astron. Astrophys.*, (1999) in prep.

[21] Funato Y., Hut P., McMillan S.L.W., Makino J., *Astron. J.*, **112** (1996) 1697

[22] Giersz M., Heggie D.C., *Monthly Notices Roy. Astron. Soc.*, **268** (1994a) 257

[23] Giersz M., Heggie D.C., *Monthly Notices Roy. Astron. Soc.*, **270** (1994b) 298

[24] Giersz M., Heggie D.C., *Monthly Notices Roy. Astron. Soc.*, **279** (1996) 1037

[25] Giersz M., Heggie D.C., *Monthly Notices Roy. Astron. Soc.*, **286** (1997) 709

[26] Giersz M., Spurzem R., *Monthly Notices Roy. Astron. Soc.*, **269** (1994) 241

[27] Goodman J., *Astrophys. J.*, **313** (1987) 576

[28] Goodman J., Heggie D.C., Hut P., *Astrophys. J.*, **415** (1993) 715

[29] Grabhorn R.P., Cohn H.N., Lugger P.M., Murphy B.W., *Astrophys. J.*, **392** (1992) 86

[30] Greengard L., Rapid Evaluation of Potential Fields in Particle Systems, MIT Press (1987)

[31] Greengard L., Rokhlin V., *Journ. Comp. Phys.*, **73** (1987) 325

[32] Heggie D.C., Giersz M., Spurzem R., Takahashi K., Dynamical simulations: methods and comparisons, in J. Andersen, ed, Highlights of Astronomy **11**, Kluwer, Dordrecht (1998) in press, Preprint astro-ph/9711191

[33] Heggie D.C., *Monthly Notices Roy. Astron. Soc.*, **206** (1984) 179

[34] Heggie D.C., Ramamani N., *Monthly Notices Roy. Astron. Soc.*, **237** (1989) 757

[35] Hénon M., *Astrophys. Space Sci.*, **14** (1971) 151

[36] Hensler G., Spurzem R., Burkert A., Trassl E., *Astron. Astrophys.*, **303** (1995) 299

[37] Hernquist L., Ostriker J.P., *Astrophys. J.*, **386** (1992) 375

[38] Hockney R.W., Eastwood J.W., Computer Simulation Using Particles, Adam Hilger, New York (1988)

[39] von Hoerner S., *Zeits. f. Astroph.*, **50** (1960) 184

[40] von Hoerner S., *Zeits. f. Astroph.*, **57** (1963) 47

[41] Hut P., *Astrophys. J.*, **403** (1993) 256

[42] Hut P., Makino J., McMillan S.L.W., *Astrophys. J.*, **443** (1995) L93

[43] Innanen K., Mikkola S., Wiegert P., *Astron. J.*, **116** (1998) 2055

[44] Klypin A., Holtzman J., "Particle-Mesh code for cosmological simulations", in astro-ph/9712217 (1997)

[45] Kandrup H.E., Mahon M.E., Smith H., *Astrophys. J.*, **428** (1994) 458

[46] Kroupa P., *Monthly Notices Roy. Astron. Soc.*, **277** (1995) 1491

[47] Kroupa P., Petr M., McCaughrean M.J., *Monthly Notices Roy. Astron. Soc.*, (1998) subm.

[48] Kustaanheimo P., Stiefel E.L., *J. Reine Angew. Math.*, **218** (1965) 204

[49] Larson R.B., *Monthly Notices Roy. Astron. Soc.*, **147** (1970) 323

[50] Laskar J., *Nature*, **338** (1989) 237

[51] Laskar J., Quinn T., Tremaine S., *Icarus*, **95** (1992) 148

[52] Lippert T., Glaessner U., Hoeber H., Ritzenhöfer G., Schilling K., Seyfried A., *Int'l J. Mod. Phys.*, **7** (1996) 485

[53] Lippert T., Seyfried A., Bode A., Schilling K., *IEEE Transact. Par. Distr. Syst.*, **9** (1998) 1

[54] Louis P.D., Spurzem R., *Monthly Notices Roy. Astron. Soc.*, **251** (1991) 408

[55] Lupton R.H., Gunn J.E., Griffin R.F., *Astron. J.*, **93** (1987) 1114

[56] Lynden-Bell D., Eggleton P.P., *Monthly Notices Roy. Astron. Soc.*, **191** (1980) 483

[57] Makino J., *Astrophys. J.*, **369** (1991) 200

[58] Makino J., *Publ. astr. Soc. Jap.*, **43** (1991) 859

[59] Makino J., *Astrophys. J.*, **471** (1996) 796

[60] Makino J., Aarseth S.J., *Publ. astr. Soc. Jap.*, **151** (1992) 44

[61] Makino J., Hut P., *Astrophys. J. Suppl.*, **68** (1988) 833

[62] Makino J., Taiji M., Scientific Simulations with Special Purpose Computers, Wiley, Weinheim (1998)

[63] Makino J., Taiji M., Ebisuzaki T., Sugimoto D., *Astrophys. J.*, **480** (1997) 432

[64] McMillan S.L.W., Hut P., *Astrophys. J.*, **467** (1996) 348

[65] Mikkola S., *Celest. Mech. Dyn. Astron.*, **67** (1997a) 145

[66] Mikkola S., *Celest. Mech. Dyn. Astron.*, **68** (1997b) 87

[67] Mikkola S., Aarseth S.J., *Celest. Mech. Dyn. Astron.*, **64** (1996) 197

[68] Mikkola S., Aarseth S.J., *New Astronomy*, **3** (1998) 309

[69] Miller R.H., *Astrophys. J.*, **140** (1964) 250

[70] Miller B.W., Whitmore B.C., Schweizer F., Fall S.M., *Astron. J.*, **114** (1997) 2381

[71] Monaghan J.J., *Ann. Rev. Astron. Astrophys.*, **30** (1992) 543

[72] Murphy B.W., Cohn H., Hut P., *Monthly Notices Roy. Astron. Soc.*, **245** (1990) 335

[73] Pearce F.R., Couchman H.M.P., *New Astronomy*, **2** (1997) 411

[74] Pfalzner S., Gibbon P., Many-Body Tree Methods in Physics, Cambridge University Press, Cambridge (1996)

[75] Portegies Zwart S.F., Hut P., Makino J., McMillan S.L.W., *Astron. Astrophys.*, (1998) subm. astro-ph/9803084

[76] Rosenbluth M.N., MacDonald W.M., Judd D.L., *Phys. Rev. 2nd Ser.*, **107** (1957) 1

[77] Spitzer L., Dynamical Evolution of Globular Clusters, Princeton Series in Astrophysics, Princeton University Press, New Jersey, USA (1987)

[78] Spurzem R., Ph.D. Thesis, Göttingen Univ., Germany (1988)

[79] Spurzem R., *Monthly Notices Roy. Astron. Soc.*, **252** (1991) 177

[80] Spurzem R., Aarseth S.J., *Monthly Notices Roy. Astron. Soc.*, **282** (1996) 19

[81] Spurzem R., Baumgardt H., *Monthly Notices Roy. Astron. Soc.*, (1998) A parallel implementation of an Aarseth N-body integrator on general and special purpose supercomputers, to be subm.

[82] Spurzem R., Takahashi K., *Monthly Notices Roy. Astron. Soc.*, **272** (1995) 772

[83] Sugimoto D., Chikada Y., Makino J., Ito T., Ebisuzaki T., Umemura M., *Nature*, **345** (1990) 33

[84] Sweatman W., *Journ. Comp. Phys.*, **111** (1994) 110

[85] Takahashi K., *Publ. astr. Soc. Jap.*, **47** (1995) 561

[86] Takahashi K., *Publ. astr. Soc. Jap.*, **48** (1996) 691

[87] Takahashi K., *Publ. astr. Soc. Jap.*, **49** (1997) 547

[88] Theis C., Spurzem R., *Astron. Astrophys.*, **341** (1999) 361

[89] Wisdom J., Holman M., *Astron. J.*, **102** (1991) 1520